Full Length Article

# An enriched environment prevents cognitive impairment in an Alzheimer's disease model by enhancing the secretion of exosomal microRNA-146a from the choroid plexus

Masako Nakano [a,*], Kenta Kubota [a,b], Shin Hashizume [a], Eiji Kobayashi [a,c], Takako S. Chikenji [a,d], Yuki Saito [a], Mineko Fujimiya [a]

[a] Department of Anatomy, Sapporo Medical University, School of Medicine, Sapporo, Hokkaido, Japan
[b] Department of Physical Therapy, Hokkaido Chitose Rehabilitation College, Chitose, Hokkaido, Japan
[c] Graduate School of Rehabilitation Science, Hokkaido Bunkyo University, Eniwa, Hokkaido, Japan
[d] Department of Health Sciences, School of Medicine, Hokkaido University, Sapporo, Hokkaido, Japan

ABSTRACT

Alzheimer's disease (AD) is characterized by the extensive deposition of amyloid-β plaques and neurofibrillary tangles. We previously found that preserved function of astrocytes is associated with cognitively normal subjects with AD pathology. Here we show that an enriched environment (EE) can prevent cognitive impairment in AD model mice by ameliorating astrocytic inflammation and increasing synaptic density in the subiculum area of the hippocampus. In AD model mice treated with an EE, increased levels of microRNA (miR)-146a and down-regulation of NF-κB were observed in the hippocampus. In addition, increased levels of interferon (IFN)-γ were seen in serum from mice exposed to an EE. In vitro, enhanced miR-146a expression was observed in exosomes derived from the choroid plexus (CP) after IFN-γ treatment. In further in vitro experiments, we transfected miR-146a into Aβ/lipopolysaccharide-induced inflammatory astrocytes and showed that miR-146a ameliorated astrocytic inflammation by down-regulating tumor necrosis factor receptor-associated factor 6 and NF-κB. The present study indicates that following an EE, exosomal miR-146a derived from the CP cells is a key factor in ameliorating astrocytic inflammation, leading to synaptogenesis and correction of cognitive impairment.

## 1. Introduction

Alzheimer's disease (AD), the most common form of dementia, impairs memory and cognitive function. The cause of AD is believed to be an accumulation of amyloid-β (Aβ) plaques and tau protein aggregates (Hardy and Selkoe, 2002; Querfurth and LaFerla, 2010). However, drugs targeting Aβ including β-secretase inhibitors and immunotherapies have resulted in negative clinical outcomes (Doody et al., 2013; Salloway et al., 2014). In contrast, several postmortem studies have revealed the presence of cognitively normal elderly people with histopathological features of AD (Neuropathology, 2001). In addition, we found that preserved astrocyte function is associated with normal cognitive function in subjects with severe accumulation of Aβ and tau in the human brain (Kobayashi et al., 2018). Furthermore, we found that enriched

environment (EE), which is a condition of large space with toys and a maze, can prevent the astroglial inflammation in a rat model of diabetes-induced cognitive impairment (Kubota et al., 2018). In this study, we hypothesized that an EE may have a positive effect on damaged astrocytes in an AD model similar to the diabetic model.

To maintain proper astrocyte function, growth factors including insulin-like growth factor I are necessary (Logan et al., 2018). The choroid plexus (CP) is known to secrete several growth factors that are taken up into the brain parenchyma (Carro et al., 2005). The CP plays a key role in supporting neuronal and astroglial function by secreting various soluble factors into the cerebrospinal fluid (CSF) (Stopa et al., 2001). Since AD patients show impaired function of the CP such as reduced secretion of soluble factors (Balusu et al., 2016a), and decreased secretion of growth factors is suggested to be associated with astrocyte dysfunction. In fact, the blockade of insulin-like growth factor I signaling in the CP is known to induce AD-like neuropathology such as amyloidosis, gliosis, and synaptic loss (Carro et al., 2006).

Moreover, decreased expression of interferon (IFN)-γ and an imbalance in Th1/Th2 cytokines in the CP area are known in an AD model

(Baruch et al., 2013, 2015). This decrease of IFN-γ acts to suppress the secretion of neurotrophic factors from the CP cells (Deczkowska et al., 2016). However, an EE is known to increase the levels of Th1-derived IFN-γ in the serum (Qi et al., 2018). Because the CP is the area of interface between the brain and the periphery (Marques and Sousa, 2015), increased serum level of IFN-γ may affect the secretion of neurotrophic factors from the CP cells.

In addition to neurotrophic factors, the CP cells is known to secrete exosomes into the CSF (Balusu et al., 2016b; Grapp et al., 2013). Exosomes are small vesicles that secreted from various cells and is known to contain various molecules such as DNA, mRNA, microRNA (miRNA) and proteins (Samanta et al., 2018). Exosomes plays a role of cell-cell communication by transferring their cargo of molecules into recipient cells (Samanta et al., 2018). Since CP cell derived exosomes are known to be taken up by astrocytes (Grapp et al., 2013), exosomal molecules are suggested to be transferred.

CP cells is known to secrete exosomal miR-146a into the CSF (Balusu et al., 2016b). miR-146a is a miRNA possessing the anti-inflammatory function, however lower levels of miR-146a in the CSF is known in AD patients (Muller et al., 2014). miRNA is a noncoding RNA of 19–24 nucleotide and known to regulate various gene expressions (Bhaskaran and Mohan, 2014). miR-146a can inhibit the expression of nuclear factor-kappa B (NF-κB) by targeting the genes of interleukin-1 receptor associated kinase 1 (IRAK1) and tumor necrosis factor receptor-associated factor 6 (TRAF6) in astrocytes (Iyer et al., 2012). We previously reported that EE treatment prevents the diabetes-induced cognitive impairment by up-regulating the exosomal level of miR-146a in serum and ameliorating the astroglial damage (Kubota et al., 2018). In addition, we found that mesenchymal stem cell (MSC) therapy also improves the cognitive impairments in AD model mice by increasing the level of miR-146a in hippocampus and inhibiting the astroglial inflammation (Nakano et al., 2020).

In this study, we hypothesized that an EE may up-regulate the level of IFN-γ in serum, enhance the secretion of exosomal miR-146a from the CP cells and ameliorate the astroglial damage in AD model.

## 2. Material and methods

### 2.1. Animals

All methods for animal experiments were performed in accordance with the approved guidelines of the Animal Experiment Committee of Sapporo Medical University (Sapporo, Japan). All experimental protocols were approved by the Animal Experiment Committee of Sapporo Medical University (approval #15–033, #17–065).

Male 5 × FAD mice (#034848) were purchased from The Jackson Laboratory (Bar Harbor, ME, USA). 5 × FAD mice are carrying five mutations: the K670 N/M671L (Swedish), I716V (Florida), and V717I (London) mutations in human APP and the M146L and L286V mutations in human PS1 (Oakley et al., 2006). Male 5 × FAD mice were crossed with WT C57BL/6 J females (Sankyo Lab Service Corp.) to obtain the needed number of mice for experiments. The temperature of the room was maintained between 21 and 24 °C, and the humidity was controlled between 50% and 70%. Animals were reared in a 12-h light/12-h dark cycle, with ad libitum access to food and water.

Every effort was performed to eliminate pain and distress. Invasive procedures were conducted using isoflurane inhalation, and the absence of the toe pinch reflex was checked for evaluation of anesthetic adequacy. At the end of the experiments, an intraperitoneal overdose injection of sodium pentobarbital (>120 mg/kg) or excess isoflurane inhalation was carried out to euthanize animals. After confirming cardiac arrest, all blood was collected from the heart of animals.

### 2.2. Housing conditions

Male WT and 5 × FAD mice were housed in a conventional cage (CC, 300 mm × 190 mm × 170 mm) starting at birth. At 3 months of age, these mice were randomly divided into (1) CC with 5–6 mice per cage or (2) environmental enrichment cage (EE, 580 mm × 400 mm × 320 mm) with 11–12 mice per cage, and then housed in either cage until 6 months old (Fig. 1a). The EE (ViewPoint, Montreal, QC, Canada) has two levels and was designed to standardize the EE for rodents. The first level of the EE has three wheels, a red tunnel, and a place for food and water. A maze was present in the second level and was regularly changed three times a week. Mice needed to go through the maze to reach both food and water. Female 5 × FAD mice were also housed in CC or EE from 3 to 6 months old age, followed by MWM. Male WT were also housed in CC with 4 mice per cage until 6 months old, then MWM was performed.

### 2.3. MWM test

The MWM test was performed as described previously (Nakano et al., 2016). A circular pool (1.2 m diameter) was filled with water (25 ± 1 °C), and several visual cues were placed around the pool. After visible platform training (day 0), hidden platform sessions were conducted four times a day (days 1–5). The time to reach the platform that set in south east (SE) and the swimming speed were measured during the hidden platform sessions. When mice did not reach the platform in 60 s, they were manually placed on the platform for 15 s. At day 6, the mice were released for 60 s into the pool in which the platform had been removed, and both crossing times of the platform and the time spent in each quadrant was recorded. Performance-incompetent mice that fail to swim or exhibit aberrant behavior are removed from the analysis of acquisition phase tests and probe trials (Weitzner et al., 2015).

Swimming strategies of mice were classified into 6 categories (Thigmotaxis, Random search, Scanning, Directed search, Focal search and Direct Swimming) as described previously (Sonobe et al., 2015). The percentage of non-spatial search (total percentage of the patterns of Thigmotaxis, Random search and Scanning) per trial was calculated during the acquisition phase in each group.

### 2.4. Immunohistochemical analysis

After the MWM test, male mice were intraperitoneally injected with sodium pentobarbital (>120 mg/kg). After detecting asystole, all blood was collected, and the mice were perfused with 0.1 M PBS through the left ventricle. Brains were removed from the skull and divided into the left and right hemispheres with a scalpel. The left hemisphere was immersed in 4% paraformaldehyde for 24 h and then placed into 15% sucrose solution. The right hemisphere was frozen immediately and stored at −80 °C for PCR analysis. The left hemispheres were sagittally cut into 20-μm thick frozen sections, and then three sections that include the area of hippocampus and CP (1.4–2.4 mm lateral from the bregma) were chosen for immunostaining.

The sections were incubated overnight at 4 °C with primary antibodies (listed in Supplementary Table 1). Secondary antibodies are listed in Supplementary Table 2. For nuclear staining, DAPI (Dojindo, Kumamoto, Japan) was used. Images were obtained with confocal laser scanning microscopy (Nikon, Tokyo, Japan).

The mean of Aβ-positive area in 200 × 200 μm fields (three fields per section × three sections), the means of number of NeuN-positive cells in 150 × 150 μm field (two fields per section × three sections), the means of intensity of synaptophysin in 200 × 200 μm field (three fields per section × three sections), the means of number of GFAP-positive cells in 310 × 310 μm (one field per section × three sections), the means of GFAP-positive area in 150 × 150 μm (three fields per section × three sections), the means of TNFα-positive area in 200 × 200 μm (three fields per section × three sections) and the means of number of Iba1-positive cells in 310 × 310 μm (one field per section × three sections) in the subiculum area were analyzed. Additionally, the subtype of Iba1-positive cells including those with smaller cell bodies ($<70$ μm$^2$) with ramified foot processes (resting microglia), larger cell bodies ($>70$ μm$^2$) with retracted branches (activated microglia), MHC class II-positive larger cell bodies
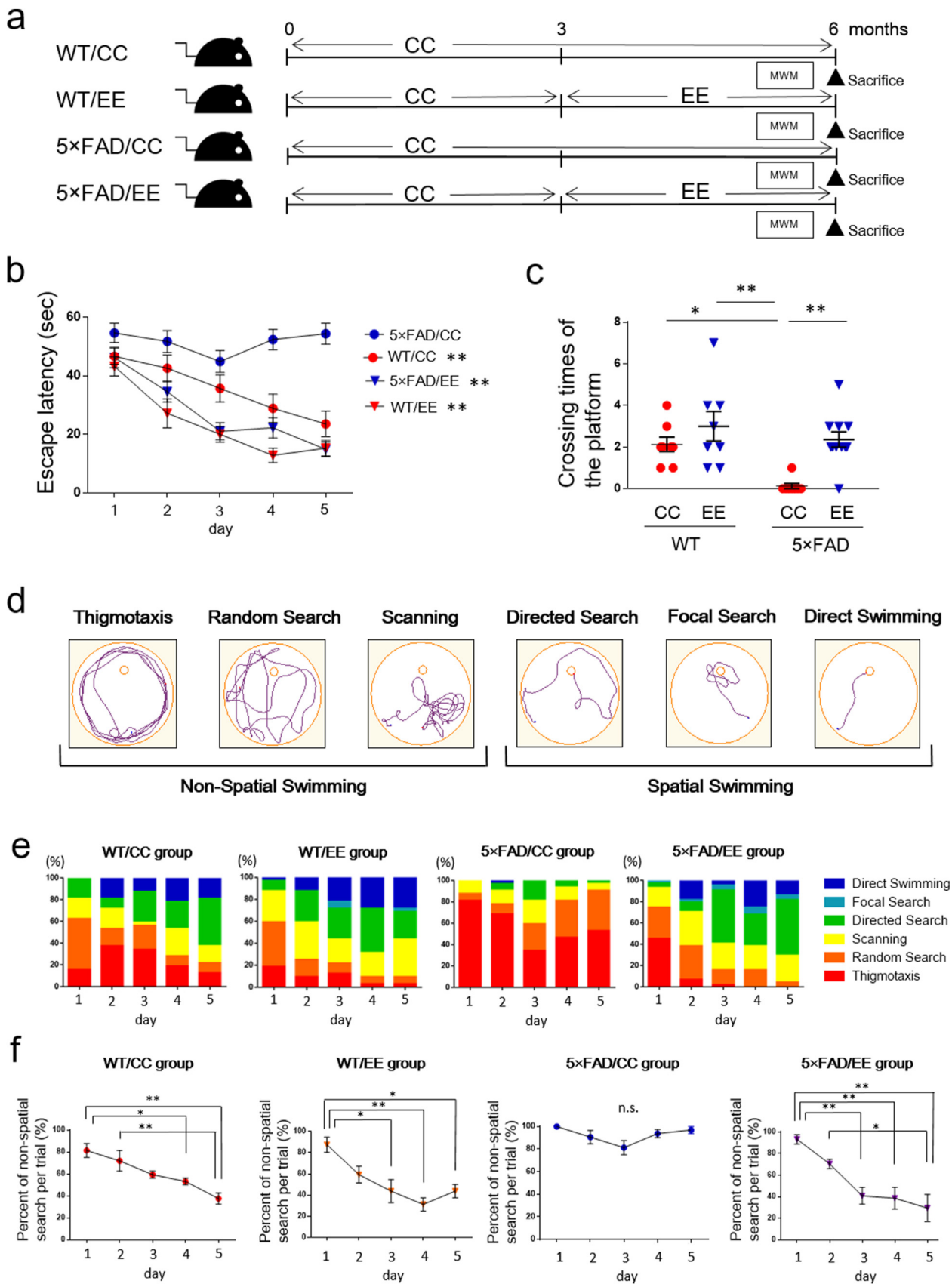
(caption on next page)

**Fig. 1. The behavioral effects of an EE in AD male model mice.** (a) Experimental protocol. WT and $5 \times$ FAD mice were housed in a CC or EE from 3 to 6 months of age. (b) The acquisition phase test of the MWM test. WT/CC (n = 8), WT/EE (n = 8), $5 \times$ FAD/CC (n = 8), $5 \times$ FAD/EE (n = 11). Values are the means of 4 trials per day $\pm$SEM. $**P < 0.01$, one-way ANOVA for repeated measures. WT/CC, $F (3.026, 21.19) = 5.895$, $P = 0.0043$; WT/EE, $F (2.431, 17.02) = 9.73$, $P = 0.0010$; $5 \times$ FAD/CC, $F (2.767, 19.37) = 1.525$, $P = 0.2408$; $5 \times$ FAD/EE, $F (2.337, 23.37) = 17.73$, $P < 0.0001$). (c) The number of platform crossing in the probe test. WT/CC (n = 8), WT/EE (n = 8), $5 \times$ FAD/CC (n = 8), $5 \times$ FAD/EE (n = 11). Values are the means $\pm$ SEM. $*P < 0.05$, $**P < 0.01$, two-way ANOVA, Tukey post-hoc test. Genotype ($F (1, 31) = 9.195$, $P = 0.0049$), Environment ($F (1, 31) = 12.83$, $P = 0.0012$), Genotype $\times$ Environment ($F (1, 31) = 2.460$, $P = 0.1267$). (d) Six categories of swimming strategies. (e) Coding color shows the percentage of swimming strategies of 4 groups per each day. (f) The percent of non-spatial search (total percentage of the patterns of Thigmotaxis, Random search and Scanning) per trial during the acquisition phase. Values are the means of 4 trials per day $\pm$ SEM. The WT/CC group (n = 8). $*P < 0.05$, $**P < 0.01$, one-way ANOVA, Bonferroni post-hoc test, $F (4, 15) = 8.292$, $P = 0.0010$. The WT/EE group (n = 8). $*P < 0.05$, $**P < 0.01$, one-way ANOVA, Bonferroni post-hoc test, $F (4, 15) = 7.579$, $P = 0.0015$. The $5 \times$ FAD/CC group (n = 8). One-way ANOVA, Bonferroni post-hoc test, $F (4, 15) = 2.650$, $P = 0.0745$. The $5 \times$ FAD/EE group (n = 11). $*P < 0.05$, $**P < 0.01$, one-way ANOVA, Bonferroni post-hoc test, $F (4, 15) = 9.808$, $P = 0.0004$. (For interpretation of the references to color in this figure legend, the reader is referred to the Web version of this article.)

with retracted branches (M1 type of activated microglia) and MMR2-positive larger cell bodies with retracted branches (M2 type of activated microglia) were counted. The intensity of TTR were analyzed in the CP area per section. Nikon NIS Elements AR software was used for all quantitative analysis.

### 2.5. Electron microscope observations

After fixation (4% paraformaldehyde), the left hemispheres were sagittally cut into 100-μm thick sections with a vibratome (VT12005, Leica, Tokyo, Japan). Then, sections that included the hippocampus (1.4–2.4 mm lateral from the bregma) were selected, and the hippocampus area was cut out with a scalpel. After fixation with 2.5% glutaraldehyde, the sections were post-fixed with 2% osmium tetroxide and embedded in epon (EPON812, TAAB Laboratories Equipment, Berks, UK). Using an ultramicrotome (RMT, Tucson, AZ, USA), ultra-thin sections (70 nm) were cut. After staining with uranyl acetate and lead citrate, sections from the subiculum area were observed by electron microscopy (H7650, HITACHI, Tokyo, Japan). The average number of synapses counted in 18 randomly selected fields at $30,000 \times$ magnification was evaluated for each mouse. Synapses were identified by the presence of a post-synaptic density.

### 2.6. miRNA and mRNA isolation from the hippocampus and quantitation

Total miRNA and mRNA were extracted from the frozen right hippocampus using the mirVana miRNA isolation kit (Thermo Fisher Scientific, Waltham, MA, USA). cDNA of targeted miRNA was synthesized according to the TaqMan MicroRNA Assay protocol (Thermo Fisher Scientific). The primers that targeted miR-146a and snoRNA 135 are listed in Supplementary Table 3. Real-time PCR was performed using an Applied Biosystems 7500 Sequence Detection system (Thermo Fisher Scientific) using TaqMan Universal PCR Mastermix II no UNG (Thermo Fisher Scientific). The relative expression was calculated using $2^{-\Delta\Delta Ct}$ using snoRNA 135 as an endogenous control.

Hippocampal mRNA was converted into cDNA using the Omniscript RT Kit (QIAGEN, Hilden, Germany). Real-time PCR was performed using an Applied Biosystems 7500 Sequence Detection system and SYBR green (Thermo Fisher Scientific). The sequences of primers are listed in Supplementary Table 4. The relative expression was calculated using $2^{-\Delta\Delta Ct}$ with GAPDH as reference gene.

### 2.7. Enzyme-linked immunosorbent assay for the serum level of IFN-γ

Serum (50 μl) from WT/CC, $5 \times$ FAD/CC and $5 \times$ FAD/EE mice was tested with the Mouse IFN-gamma Quantikine ELISA Kit (R&D Systems, Minneapolis, MN, USA), according to the manufacturer's protocol.

### 2.8. Isolation of exosomal miRNA from CP-CM after addition of recombinant proteins

The rat CP cell line (The European Collection of Authenticated Cell Cultures, London, UK) were used for culturing. CP cells were seeded at a density of $0.8 \times 10^4$ cells/cm$^2$ in a 24-well plate coated with type 1 collagen (Corning, Corning, NY, USA). Cells were cultured in DMEM/F-12 (Sigma-Aldrich, Saint Louis, MO, USA), 10% FBS (CCB, NICHIREI BIOSCIENCE, Tokyo, Japan), 10 mg/ml recombinant rat epidermal growth factor protein (R&D Systems), 1% Insulin/Transferrin/Selenium Solution (Thermo Fisher Scientific), and 1% penicillin streptomycin (PS) (Thermo Fisher Scientific) (Battle et al., 2000). Cells were maintained in a 5% $CO_2$ incubator at 37 °C. At 3 days after seeding when each cultured cell type had reached 90–100% confluence, the conventional medium was replaced with 10% EXO-FBS-50A-1 (System Biosciences, Palo Alto, CA, USA) medium with several concentrations of recombinant rat IFN-γ (0 or 0.5 ng/ml; R&D Systems). At 24 h after incubation, the culture media were collected and the exosomes were isolated using the Mag-Capture Exosome Isolation Kit PS (FUJIFILM Wako Pure Chemical Corp, Osaka, Japan).

miRNA isolation, cDNA synthesis, and RT-PCR were performed as described above. The relative expression of miR-146a was calculated using $2^{-\Delta\Delta Ct}$ with cel-miR-39 as an external spiked control.

### 2.9. Isolation and culture of primary rat astrocytes

Hippocampal tissues of neonatal SD rats (1 or 2 days old) were isolated after inhalation of excessive isoflurane, as described previously (Schulte-Herbruggen et al., 2007). Briefly, cells of hippocampal tissues were seeded at a density of $1.5 \times 10^5$ cells/cm$^2$ in poly-L-lysine (Sigma)-coated dishes. DMEM/F-12 with 10% FBS and 1% PS was used as the culture medium. The medium was first changed 24 h after seeding and then twice weekly. The culture dishes were shaken at 200 rpm overnight 7–8 days after seeding. Then, cells that remained attached were trypsinized and seeded at $5.3 \times 10^4$ cells/cm$^2$ in poly-L-lysine-coated 24-well plates or four-well chamber slides (Thermo Fisher Scientific). We confirmed that more than 95% of cultured cells were astrocytes.

### 2.10. Transfection of rat astrocytes

When the cells reached 60–70% confluence, they were transfected with 20 nM miR-146a mimic (QIAGEN). Hiperdect transfection reagent (QIAGEN) was used for transfection, according to the manufacturer's instructions. After 24 h, 1 μM Aβ fibrils and 250 ng/ml LPS (Thermo Fisher Scientific) were added and incubated for 6 h. Then, RNA was extracted using TRI Reagent (Molecular Research Center, Cincinnati, OH, USA) or cells were fixed in 4% paraformaldehyde for 1 h at 4 °C for immunocytochemistry, after washing with PBS. For Aβ fibril formation, Aβ$_{1-42}$ peptide (Peptide Institute Inc., Osaka, Japan) was dissolved in sterile water at a concentration of 1 mM, and then incubated for 5 days at 37 °C (Cordle and Landreth, 2005).

### 2.11. Immunohistochemical analysis of cultured astrocytes

The cells on chamber slides were incubated with primary antibodies overnight at 4 °C. Primary and secondary antibodies are listed in Supplementary Tables 1 and 2. After obtaining images with Nikon confocal laser scanning microscopy, the GFAP-positive area per cell and the TNFα-

positive area per each cell were analyzed in 50 randomly selected cells/ group. The nucleus/cytoplasm ratio of NF-κB (NF-κB positive area in nucleus divided by NF-κB positive area in cytoplasm) were analyzed in 8 randomly selected cells/group.

### 2.12. Quantitative RT-PCR of cultured astrocytes

mRNA was converted into cDNA using the Omniscript RT Kit. Real-time PCR was performed using an Applied Biosystems 7500 Sequence Detection system and SYBR green. The sequences of primers are listed in Supplementary Table 5. The relative expression was calculated using $2^{-\Delta\Delta Ct}$ with GAPDH as the reference gene.

### 2.13. Statistical analysis

Data were expressed as the means ± standard error of the mean (SEM). Statistical analysis was performed using the unpaired $t$-test or one-way analysis of variance (ANOVA) followed by the Tukey test for post-hoc comparisons between groups. When two factors were assessed, two-way ANOVA with the Tukey test was carried out. For the acquisition phase of MWM, one-way repeated measure ANOVA or two-way of repeated measure ANOVA followed by Bonferroni was performed. To evaluate the relationship between immunohistochemical results and cognitive functions, pearson's correlation coefficient was used. GraphPad Prism 6.0 (GraphPad Software Inc., San Diego, CA, USA) was used for statistical analysis, and differences were considered significant at $P < 0.05$.
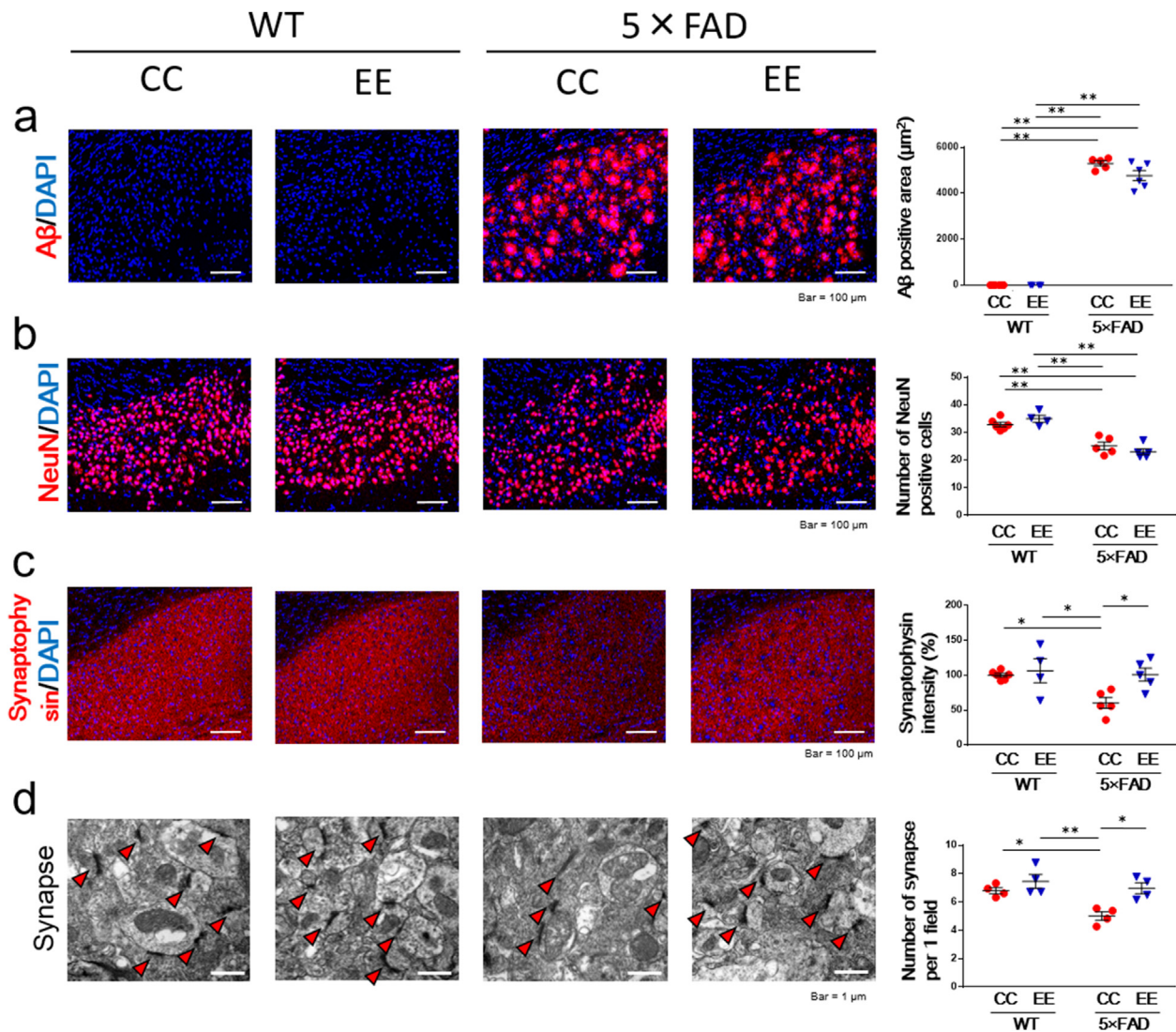


Fig. 2. Histological analysis of Aβ, neuron and synapse in the subiculum area in an EE-treated mice. (a) The Aβ-positive area. WT/CC (n = 6), WT/EE (n = 4), 5 × FAD/CC (n = 5), 5 × FAD/EE (n = 6). Values are the means ± SEM. **$P < 0.01$, two-way ANOVA, Tukey post-hoc test. Genotype ($F$ (1, 17) = 1310, $P < 0.0001$), Environment ($F$ (1, 17) = 3.623, $P = 0.0740$), Genotype × Environment ($F$ (1, 17) = 3.623, $P = 0.0740$). (b) The number of NeuN-positive cells. WT/CC (n = 6), WT/EE (n = 4), 5 × FAD/CC (n = 5), 5 × FAD/EE (n = 5). Values are the means ± SEM. **$P < 0.01$, two-way ANOVA, Tukey post-hoc test. Genotype ($F$ (1, 16) = 75.05, $P < 0.0001$), Environment ($F$ (1, 16) = 4.860*e$^{-6}$, $P = 0.9983$), Genotype × Environment ($F$ (1, 16) = 3.505, $P = 0.0796$). (c) The intensity of synaptophysin. WT/CC (n = 6), WT/EE (n = 4), 5 × FAD/CC (n = 5), 5 × FAD/EE (n = 5). Values are the means ± SEM. *$P < 0.05$, two-way ANOVA, Tukey post-hoc test. Genotype ($F$ (1, 16) = 6.054, $P = 0.0256$), Environment ($F$ (1, 16) = 6.525, $P = 0.0212$), Genotype × Environment ($F$ (1, 16) = 3.445, $P = 0.0820$). (d) The evaluation of synaptic number by electron microscopic study. Synapses were identified by the presence of a post-synaptic density (red arrowheads). WT/CC (n = 4), WT/EE (n = 4), 5 × FAD/CC (n = 4), 5 × FAD/EE (n = 4). Values are the means ± SEM. *$P < 0.05$, **$P < 0.01$, two-way ANOVA, Tukey post-hoc test. Genotype ($F$ (1, 12) = 10.11, $P = 0.0079$), Environment ($F$ (1, 12) = 13.29, $P = 0.0034$), Genotype × Environment ($F$ (1, 12) = 3.321, $P = 0.0934$). (For interpretation of the references to color in this figure legend, the reader is referred to the Web version of this article.)

## 3. Results

### 3.1. An EE prevented learning and memory impairment in 5 × FAD mice

In 5 × FAD mice, no learning and memory impairment was observed at 5 months of age (Suppl. Fig. 1a), but was observed in 6-month-old mice (Suppl. Fig. 1b). To investigate whether an EE can prevent cognitive impairment, 5 × FAD male mice were housed in a conventional cage (CC) or an EE for 3 months, from 3 to 6 months of age (Fig. 1a). MWM tests were performed at the end of CC or EE housing at 6 months old, and then mice were sacrificed for additional analysis. In the acquisition phase of the MWM test, WT/CC, WT/EE and 5 × FAD/EE group showed the shorten escape latency, however 5 × FAD/CC group did not show the shorten escape latency (Fig. 1b). In addition, the escape latency of the 5 × FAD/CC group exhibited longer time than both the WT/CC and WT/EE groups, and this time was shortened in the 5 × FAD/EE group, at day 4 and 5 (Suppl. Fig. 2d and e). In the probe test, the number of platform crossing in 5 × FAD/CC group was significantly lower compared to the WT/CC and WT/EE group, and this decrease was prevented in the 5 × FAD/EE group (Fig. 1c). In addition, the time percentage in target area

(South East: SE) was not significantly different from that of the other three areas in 5 × FAD/CC group (Suppl. Fig. 3c). However, the time percentage in target area (SE) was significantly higher than that of the other three areas in 5 × FAD/EE group (Suppl. Fig. 3d). No difference was found in the swimming speed among the four experimental groups (WT/CC; $0.1631 \pm 0.0116$ m s$^{-1}$, WT/EE; $0.1888 \pm 0.0104$ m s$^{-1}$, 5 × FAD/CC; $0.1500 \pm 0.0094$ m s$^{-1}$, 5 × FAD/EE; $0.1545 \pm 0.0140$ m s$^{-1}$).

For the analysis of movement patterns of mice in the acquisition phase, we classified each trial into 6 strategies (1) Thigmotaxis, (2) Random search, (3) Scanning, (4) Directed search, (5) Focal search and (6) Direct swimming (Sonobe et al., 2015) (Fig. 1d). The former three are non-spatial swimming, and the latter three are spatial swimming (Sonobe et al., 2015). The percent of non-spatial swimming was significantly decreased in the WT/CC, WT/EE and 5 × FAD/EE groups during the acquisition phase, however that of the 5 × FAD/CC group was not changed (Fig. 1e and f).

In this study, we also compared the cognitive function between the WT/CC groups housed in 5–6 mice per cage and the WT/CC group housed in 4 mice per cage. However, there was no difference between two groups in the result of escape latencies and the number of platform
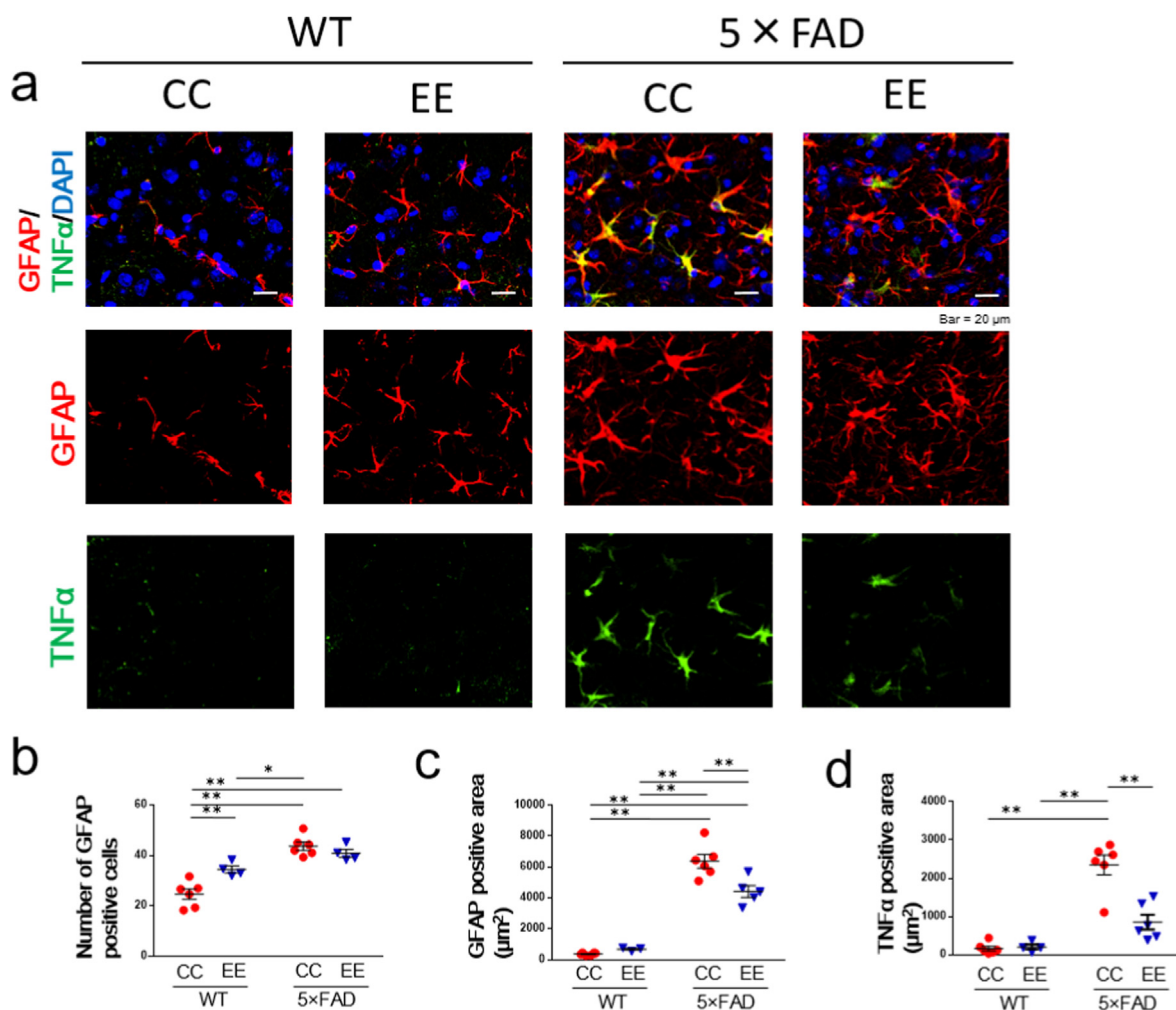


**Fig. 3. Immunohistochemical analysis of astrocyte in the subiculum area in an EE-treated mice.** (a) Representative image of GFAP and TNFα. (b) The number of GFAP-positive cells. WT/CC (n = 6), WT/EE (n = 4), 5 × FAD/CC (n = 5), 5 × FAD/EE (n = 4). Values are the means ± SEM. *$P < 0.05$, **$P < 0.01$, two-way ANOVA, Tukey post-hoc test. Genotype ($F (1, 16) = 48.09$, $P < 0.0001$), Environment ($F (1, 16) = 3.702$, $P = 0.0723$), Genotype × Environment ($F (1, 16) = 11.90$, $P = 0.0033$). (c) The GFAP-positive area. WT/CC (n = 6), WT/EE (n = 3), 5 × FAD/CC (n = 6), 5 × FAD/EE (n = 5). Values are the means ± SEM. **$P < 0.01$, two-way ANOVA, Tukey post-hoc test. Genotype ($F (1, 16) = 203.1$, $P < 0.0001$), Environment ($F (1, 16) = 5.721$, $P = 0.0294$), Genotype × Environment ($F (1, 16) = 10.90$, $P = 0.0045$). (d) The TNFα-positive area co-localized with GFAP. WT/CC (n = 6), WT/EE (n = 4), 5 × FAD/CC (n = 6), 5 × FAD/EE (n = 6). Values are the means ± SEM. **$P < 0.01$, two-way ANOVA, Tukey post-hoc test. Genotype ($F (1, 18) = 58.83$, $P < 0.0001$), Environment ($F (1, 18) = 15.41$, $P = 0.0010$), Genotype × Environment ($F (1, 18) = 17.27$, $P = 0.0006$).

crossing (Suppl. Fig. 4a and b). In addition to 5 × FAD male mice, we also housed 5 × FAD female mice in CC or EE from 3 to 6 months of age. Similar to 5 × FAD male mice, the escape latency of the 5 × FAD/EE female mice was significantly shortened compared to the 5 × FAD/CC female mice at day 2, 4 and 5 (Suppl. Fig. 5a). The number of platform crossing in the 5 × FAD/EE female group was significantly higher compared to the 5 × FAD/CC female group (Suppl. Fig. 5a). In addition, the time percentage in target area (SE) was not significantly different from that of the other three areas in 5 × FAD/CC female group. However, the time percentage in target area (SE) was significantly higher than that of the other three areas in 5 × FAD/EE female group (Suppl. Fig. 5b). No difference was found in the swimming speed among the 2 experimental groups (5 × FAD/CC; 0.1674 ± 0.0142 m s$^{-1}$, 5 × FAD/EE; 0.1781 ± 0.0109 m s$^{-1}$).

### 3.2. An EE id did not affect the area of Aβ or neuronal loss in AD model mice

In the next studies, the mechanisms of how an EE prevents cognitive impairment in AD male model mice were examined. The area of Aβ was significantly higher in the 5 × FAD/CC group than the WT/CC and WT/EE groups, and this increase was not ameliorated in the 5 × FAD/EE group (Fig. 2a).

The number of neurons in the subiculum region was also compared in mice treated with an EE (Fig. 2b). The number of neurons was significantly lower in the 5 × FAD/CC group than the WT/CC and WT/EE groups, and this decrease was not prevented in the 5 × FAD/EE group

(Fig. 2b). Neither the area of Aβ nor the number of neurons were not correlated with cognitive function (Suppl. Fig. 6a and b).

### 3.3. An EE increased the synaptic density in AD model mice

The effects of an EE on synaptic density were examined by staining for the synaptic marker, synaptophysin, in the subiculum. The intensity of synaptophysin was significantly decreased in the 5 × FAD/CC group compared to the WT/CC and WT/EE groups, and this decrease was prevented in the 5 × FAD/EE group (Fig. 2c). In addition, the intensity of synaptophysin was positively correlated with cognitive function (Suppl. Fig. 6c). To evaluate synaptic density in detail, we counted the number of synapses in the subiculum area as seen with electron microscopy. The number of synapses was significantly decreased in the 5 × FAD/CC group compared to the WT/CC and WT/EE groups, and this decrease was prevented in the 5 × FAD/EE group (Fig. 2d).

### 3.4. An EE decreased the glial fibrillary acidic protein (GFAP)- and tumor necrosis factor (TNF)α-positive areas in astrocytes in AD model mice

Astrocytic characteristics in the subiculum region were examined by staining for GFAP and TNFα in mice treated with an EE (Fig. 3a). The number of GFAP-positive cells in the WT/EE group was significantly higher than in the WT/CC group, and the 5 × FAD/CC group also showed a significant increase in GFAP-positive cells compared to the WT/CC and WT/EE groups. However, this increase in the 5 × FAD/CC group was not ameliorated in the 5 × FAD/EE group (Fig. 3b).
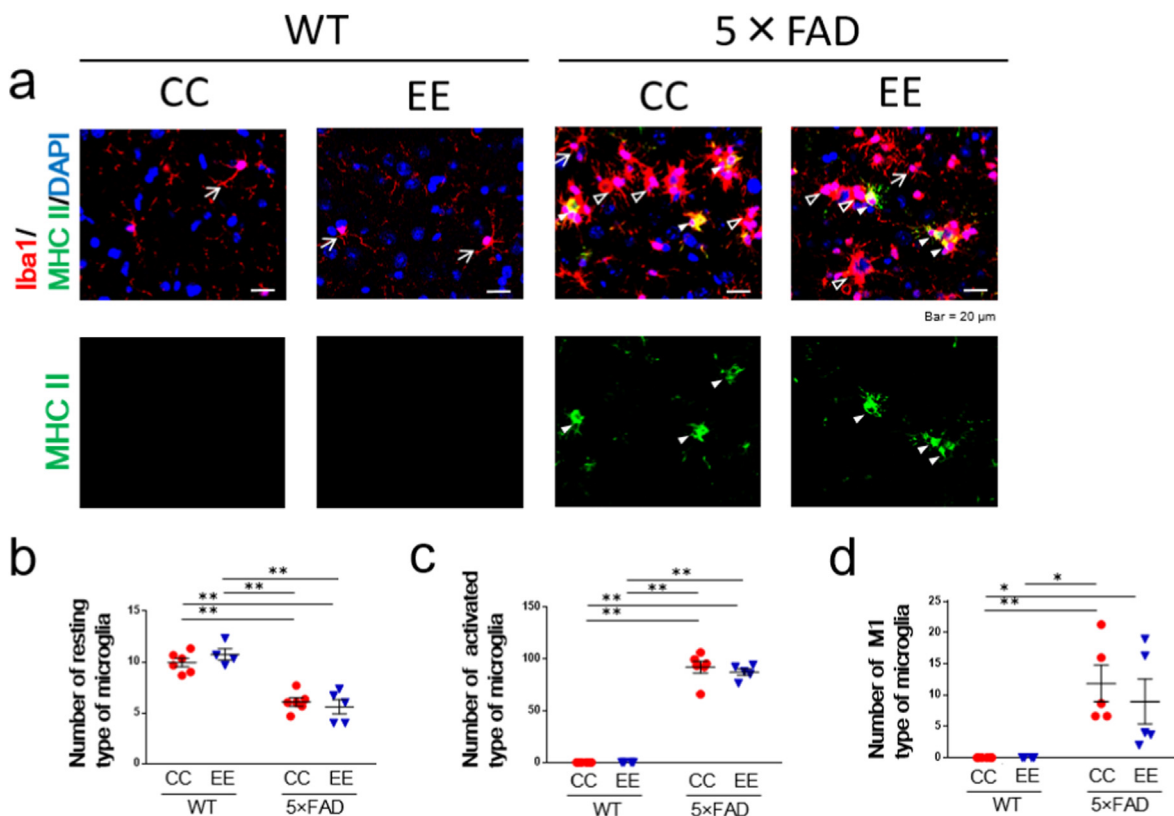


**Fig. 4. Immunohistochemical analysis of microglia in the subiculum area in an EE-treated mice.** (a) Representative image of Iba1 and MHC II. (b) The number of the resting type of microglia (arrows). WT/CC (n = 6), WT/EE (n = 4), 5 × FAD/CC (n = 6), 5 × FAD/EE (n = 5). Values are the means ± SEM. **$P < 0.01$, two-way ANOVA, Tukey post-hoc test. Genotype ($F (1, 17) = 76.40$, $P < 0.0001$), Environment ($F (1, 17) = 0.1135$, $P = 0.7403$), Genotype × Environment ($F (1, 17) = 1.489$, $P = 0.2391$). (c) The number of the activated type of microglia (white and black arrowheads). WT/CC (n = 6), WT/EE (n = 4), 5 × FAD/CC (n = 6), 5 × FAD/EE (n = 5). Values are the means ± SEM. **$P < 0.01$, two-way ANOVA, Tukey post-hoc test. Genotype ($F (1, 17) = 605.3$, $P < 0.0001$), Environment ($F (1, 17) = 0.4619$, $P = 0.5059$), Genotype × Environment ($F (1, 17) = 0.4619$, $P = 0.5059$). (d) The number of the M1 type of microglia (white arrowheads). WT/CC (n = 6), WT/EE (n = 4), 5 × FAD/CC (n = 5), 5 × FAD/EE (n = 5). Values are the means ± SEM. *$P < 0.05$, **$P < 0.01$, two-way ANOVA, Tukey post-hoc test. Genotype ($F (1, 16) = 19.99$, $P = 0.0004$), Environment ($F (1, 16) = 0.3794$, $P = 0.5466$), Genotype × Environment ($F (1, 16) = 0.3794$, $P = 0.5466$).
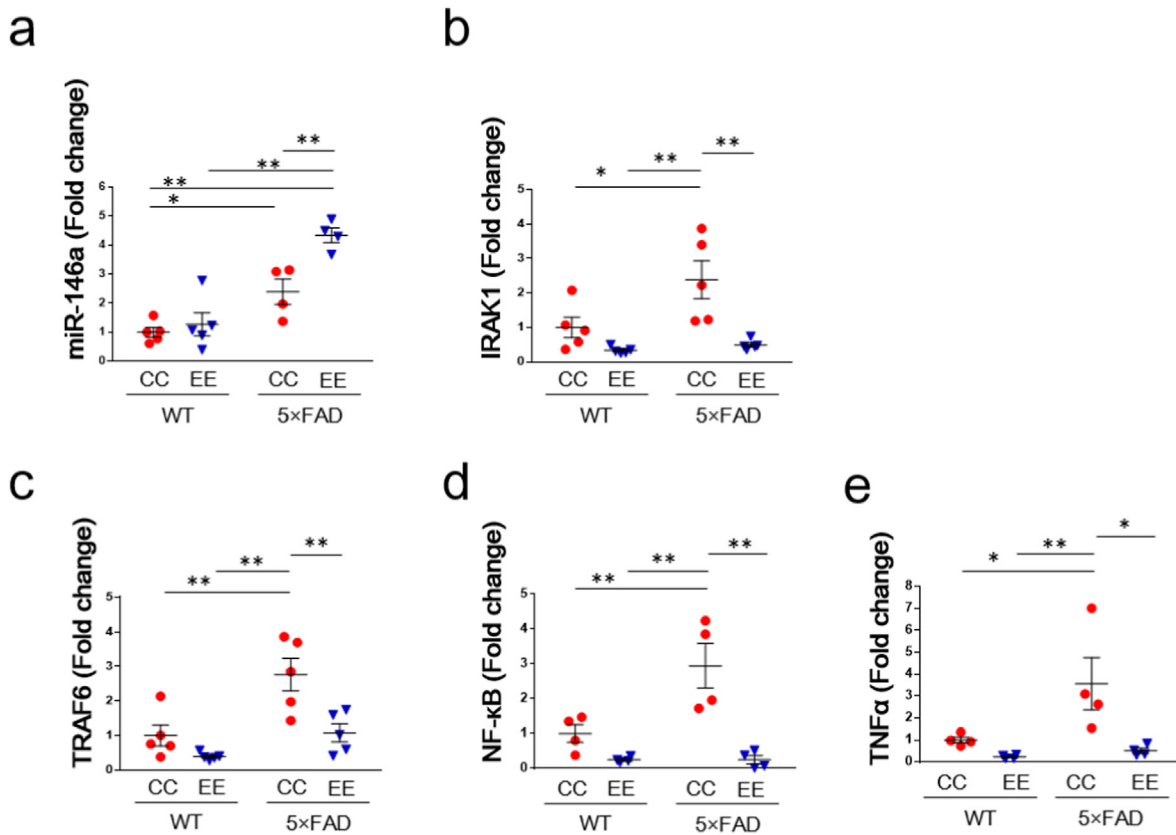
Fig. 5. Analysis of miRNA and mRNA in the hippocampus. (a) The expression of miR-146a. WT/CC (n = 5), WT/EE (n = 5), 5 × FAD/CC (n = 4), 5 × FAD/EE (n = 4). Values are the means ± SEM. *$P < 0.05$, **$P < 0.01$, two-way ANOVA, Tukey post-hoc test. Genotype ($F$ (1, 14) = 45.57, $P < 0.0001$), Environment ($F$ (1, 14) = 11.31, $P = 0.0046$), Genotype × Environment ($F$ (1, 14) = 6.441, $P = 0.0237$). (b) The expression of IRAK1. WT/CC (n = 5), WT/EE (n = 5), 5 × FAD/CC (n = 5), 5 × FAD/EE (n = 5). Values are the means ± SEM. *$P < 0.05$, **$P < 0.01$, two-way ANOVA, Tukey post-hoc test. Genotype ($F$ (1, 16) = 5.980, $P = 0.0264$), Environment ($F$ (1, 16) = 16.54, $P = 0.0009$), Genotype × Environment ($F$ (1, 16) = 3.815, $P = 0.0685$). (c) The expression of TRAF6. WT/CC (n = 5), WT/EE (n = 5), 5 × FAD/CC (n = 5), 5 × FAD/EE (n = 5). Values are the means ± SEM. **$P < 0.01$, two-way ANOVA, Tukey post-hoc test. Genotype ($F$ (1, 16) = 15.50, $P = 0.0012$), Environment ($F$ (1, 16) = 13.61, $P = 0.0020$), Genotype × Environment ($F$ (1, 16) = 3.048, $P = 0.1000$). (d) The expression of NF-κB. WT/CC (n = 4), WT/EE (n = 4), 5 × FAD/CC (n = 4), 5 × FAD/EE (n = 4). Values are the means ± SEM. **$P < 0.01$, two-way ANOVA, Tukey post-hoc test. Genotype ($F$ (1, 12) = 7.648, $P = 0.0171$), Environment ($F$ (1, 12) = 24.06, $P = 0.0004$), Genotype × Environment ($F$ (1, 12) = 7.653, $P = 0.0171$). (e) The expression of TNFα. WT/CC (n = 4), WT/EE (n = 4), 5 × FAD/CC (n = 4), 5 × FAD/EE (n = 4). Values are the means ± SEM. **$P < 0.05$, **$P < 0.01$, two-way ANOVA, Tukey post-hoc test. Genotype ($F$ (1, 12) = 5.559, $P = 0.0362$), Environment ($F$ (1, 12) = 10.06, $P = 0.0080$), Genotype × Environment ($F$ (1, 12) = 3.634, $P = 0.0808$).

In contrast, the GFAP-positive area was significantly higher in the 5 × FAD/CC group than the WT/CC and WT/EE groups, and this increase was decreased in the 5 × FAD/EE group (Fig. 3c). Additionally, the TNFα-positive area that co-localized with GFAP was significantly higher in the 5 × FAD/CC group than the WT/CC and WT/EE groups, and this increase was ameliorated in the 5 × FAD/EE group (Fig. 3d). Furthermore, both the GFAP-positive area and TNFα-positive area were negatively correlated with cognitive function (Suppl. Fig. 6e and f).

### 3.5. An EE did not decrease the M1 type of activated microglia in AD model mice

Microglial characteristics in the subiculum region were examined by staining for Iba1 and major histocompatibility complex (MHC) class II in mice treated with an EE (Fig. 4a).

Resting microglia and activated microglia can be distinguished by morphological differences. The former are characterized by a small cell body with multiple thin processes, and the latter show enlarged cell bodies with retracted processes (Fan et al., 2017). The number of resting microglia was significantly lower in the 5 × FAD/CC group than the WT/CC and WT/EE group, and this decrease was not ameliorated in the 5 × FAD/EE group (Fig. 4b).

In contrast, the number of activated microglia was significantly higher in the 5 × FAD/CC group than the WT/CC and WT/EE groups, and this increase was not inhibited in the 5 × FAD/EE group (Fig. 4c). The number of the M1 type of activated microglia, which are positive for MHC class II, was significantly higher in the 5 × FAD/CC group than the WT/CC and WT/EE groups, but this increase was not inhibited in the 5 × FAD/EE group (Fig. 4d). We also evaluated the number of the M2 type of activated microglia by staining macrophage mannose receptor 1 (MMR). The number of the M2 type of activated microglia was significantly higher in the 5 × FAD/CC group than the WT/CC and WT/EE groups, however this increase was not inhibited in the 5 × FAD/EE group (Suppl. Fig. 7).

### 3.6. The expression of miR-146a, IRAK1, TRAF6, NF-κB and TNFα in the hippocampus of AD model mice treated with an EE

To examine hippocampal expression of miR-146a, IRAK1, TRAF6, NF-κB and TNFα, miRNA or the corresponding mRNA was analyzed in AD model mice treated with an EE. The expression of miR-146a in the hippocampus was significantly increased in the 5 × FAD/CC group compared to the WT/CC groups (Fig. 5a). Moreover, the expression of miR-146a in the hippocampus was significantly increased in the 5 ×
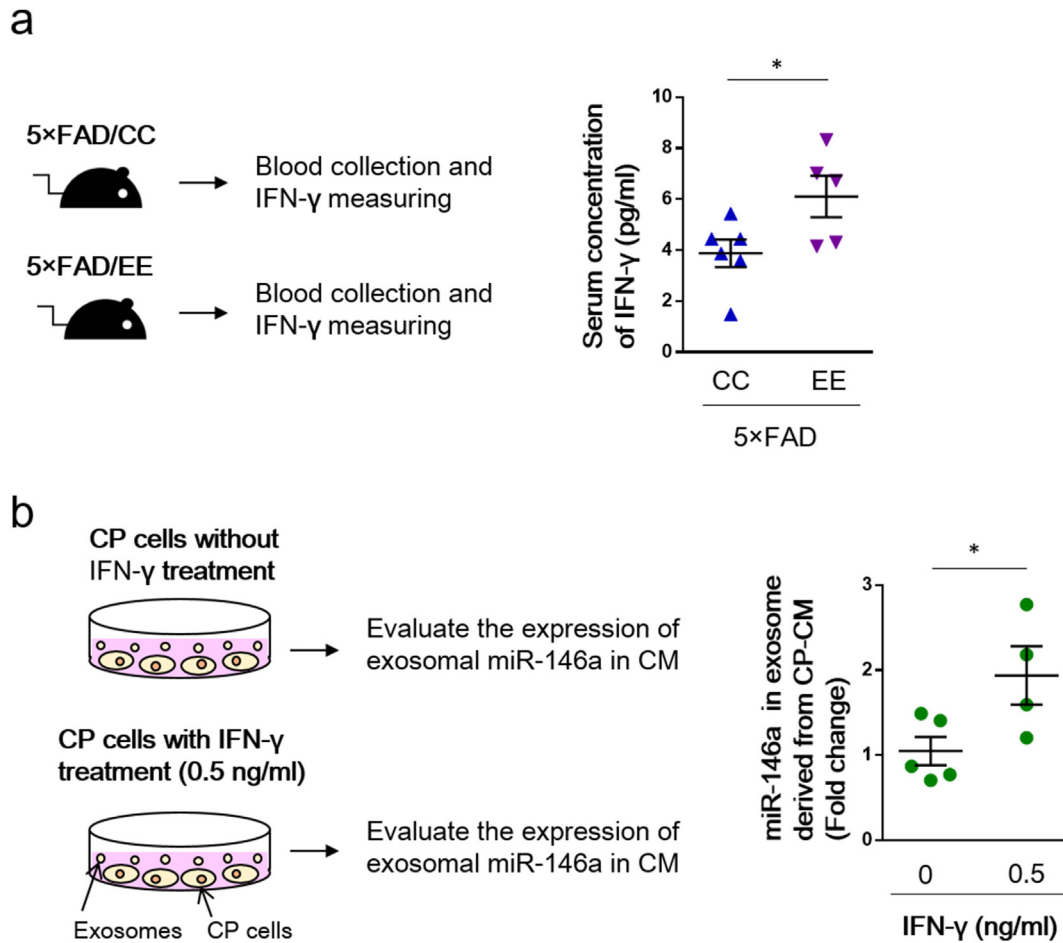
Fig. 6. Analysis of serum level of IFN-γ and exosomal miRNA-146a from CP-CM. (a) The serum level of IFN-γ was measured after the blood collections from 5 × FAD/CC and 5 × FAD/EE mice. 5 × FAD/CC (n = 6), 5 × FAD/EE (n = 5). Values are the means ± SEM. *P < 0.05, unpaired t-test. (b) The expression of exosomal miR-146a was evaluated in the conditioned medium (CM) of choroid plexus (CP) cells after IFN-γ stimulation. IFN-γ 0 ng/ml (n = 5), IFN-γ 0.5 ng/ml (n = 4). Values are the means ± SEM. *P < 0.05, unpaired t-test.

FAD/EE group compared to the 5 × FAD/CC group. The expression of both IRAK1 and TRAF6 in the hippocampus was significantly increased in the 5 × FAD/CC group compared to the WT/CC and WT/EE groups, and these increases were ameliorated in the 5 × FAD/EE group (Fig. 5b and c). Similarly, the expression of NF-κB and TNFα in the hippocampus was significantly increased in the 5 × FAD/CC group compared to the WT/CC and WT/EE groups, and this increase was ameliorated in the 5 × FAD/EE group (Fig. 5d and e).

### 3.7. IFN-γ stimulated the CP and up-regulated the level of miR-146a in exosomes derived from the CP

The serum concentration of IFN-γ was measured after the collection of blood from the 5 × FAD/CC and 5 × FAD/EE group (Fig. 6a). The serum concentration of IFN-γ in the 5 × FAD/EE group was significantly higher than that of the 5 × FAD/CC group (Fig. 6a). To evaluate whether the serum concentration of IFN-γ differs depending on genotype, we measured it from the serum of the WT/CC and 5 × FAD/CC group. However, no significant difference was observed in the serum concentration of IFN-γ between the WT/CC group and 5 × FAD/CC group (Suppl. Fig. 8).

To examine whether the increased level of IFN-γ effects on the secretion of exosomal miR-146a from the CP cells, recombinant IFN-γ was added to cultured CP cells in vitro (Fig. 6b). When recombinant IFN-γ was added at a concentration of 0 or 0.5 ng/ml to CP cells, the exosomal miR-146a in the CP-conditioned medium (CM) of the 0.5 ng/ml IFN-γ

group was significantly higher than that of the 0 ng/ml IFN-γ group at 24 h after addition (Fig. 6b).

### 3.8. Increased expression of miR-146a exerted anti-inflammatory effects on astrocytes in AD-like conditions

To examine whether the increased level of miR-146a in the hippocampus has anti-inflammatory effects on astrocytes in AD-like conditions, miR-146a was transfected into astrocytes and stimulated with 1 μM Aβ fibrils and 250 ng/ml lipopolysaccharide (LPS) to mimic AD conditions (Fig. 7a). After staining with cultured astrocytes with GFAP and TNFα, no difference was found in the GFAP-positive area per cell among the four groups: Control, Control + miR-146a, Aβ/LPS, and Aβ/LPS + miR-146a groups (Fig. 7b). On the other hand, the percentage of the TNF-α-positive area per cell was significantly increased in the Aβ/LPS group, whereas this increase was significantly decreased in the Aβ/LPS + miR-146a group (Fig. 7b). No difference was found in the gene expression of IRAK1 among the four groups. However, the gene expression of TRAF6 was significantly lower in the Aβ/LPS + miR-146a group than in the Aβ/LPS group (Fig. 7c). On the other hand, the gene expression of NF-κB was significantly higher in the Aβ/LPS group than in the Control and Control + miR-146a groups, whereas the gene expression of NF-κB in the Aβ/LPS + miR-146a group was significantly lower than that in the Aβ/LPS group (Fig. 7c).

Additionally, we evaluated the distribution of NF-κB in protein level in cultured astrocytes (Suppl. Fig. 9). The nucleus/cytoplasm ratio of NF-
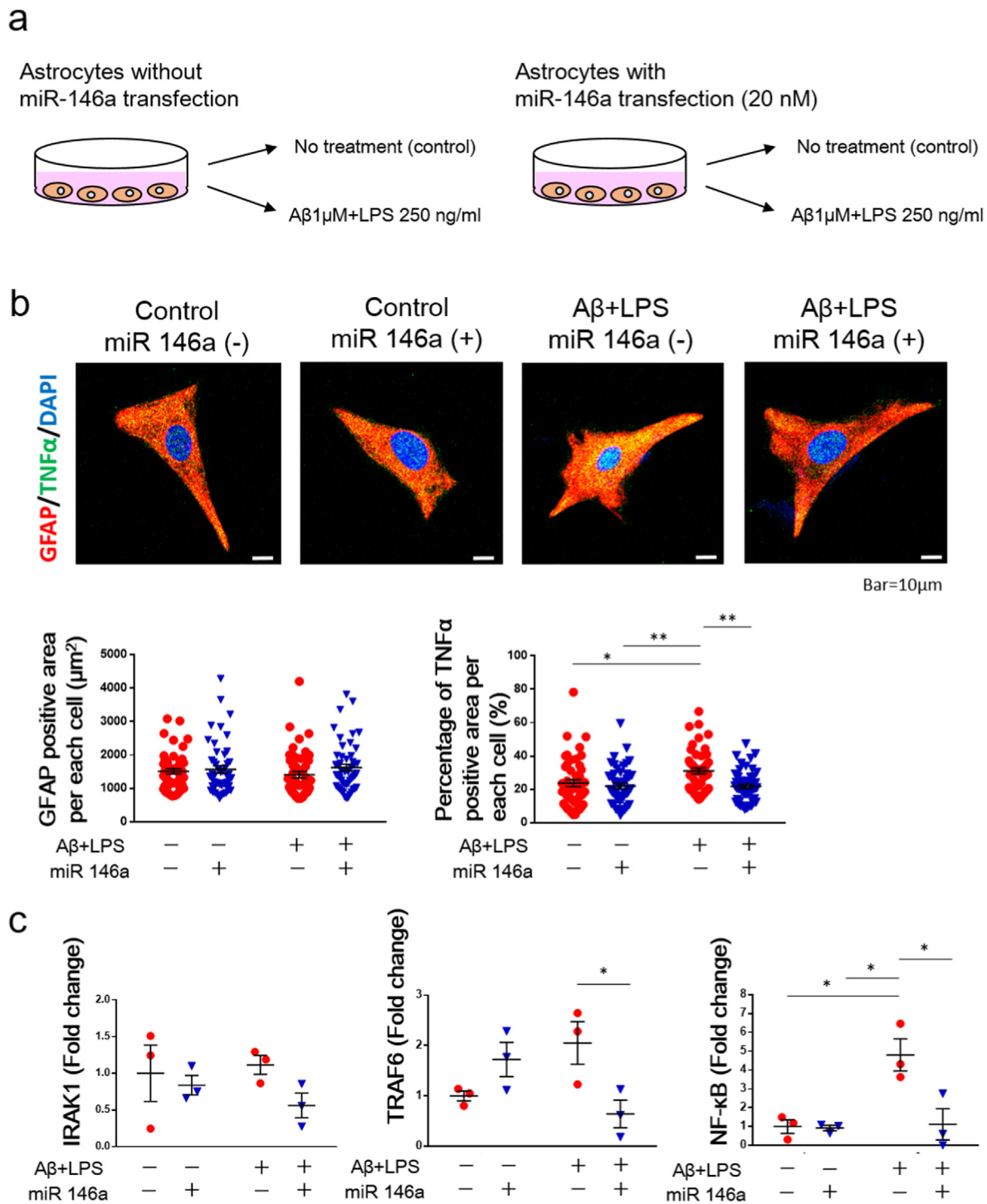
**Fig. 7. Analysis of cultured astrocytes transfected with miR-146a.** (a) To examine whether the increased level of miR-146a has anti-inflammatory effects on astrocytes, miR-146a was transfected into astrocytes and stimulated with 1 μM Aβ fibrils and 250 ng/ml lipopolysaccharide (LPS) to mimic AD conditions. (b) The GFAP-positive area per cell. n = 50 per group. Values are the means ± SEM. Two-way ANOVA, Tukey post-hoc test. miR-146a ($F$ (1, 196) = 1.915, $P$ = 0.1680), Aβ/LPS ($F$ (1, 196) = 0.05842, $P$ = 0.8093), miR-146a × Aβ/LPS ($F$ (1, 196) = 0.5840, $P$ = 0.4457). The percentage of TNFα-positive area per cell. n = 50 per group. Values are the means ± SEM.*$P$ < 0.05, **$P$ < 0.01, two-way ANOVA, Tukey post-hoc test. miR-146a ($F$ (1, 196) = 10.62 $P$ = 0.0013), Aβ/LPS ($F$ (1, 196) = 4.442, $P$ = 0.0363), miR-146a × Aβ/LPS ($F$ (1, 196) = 4.842, $P$ = 0.0289). (c) The gene expression of IRAK1. n = 3 per group. Values are the means ± SEM. Two-way ANOVA, Tukey post-hoc test. miR-146a ($F$ (1, 8) = 2.431, $P$ = 0.1571), Aβ/LPS ($F$ (1, 8) = 0.1235, $P$ = 0.7343), miR-146a × Aβ/LPS ($F$ (1, 8) = 0.7256, $P$ = 0.4191). The gene expression of TRAF6. n = 3 per group. Values are the means ± SEM. *$P$ < 0.05, two-way ANOVA, Tukey post-hoc test. miR-146a ($F$ (1, 8) = 1.227, $P$ = 0.3001), Aβ/LPS ($F$ (1, 8) = 0.001938, $P$ = 0.9660), miR-146a × Aβ/LPS ($F$ (1, 8) = 11.95, $P$ = 0.0086). The gene expression of NF-κB. n = 3 per group. Values are the means ± SEM. *$P$ < 0.05, two-way ANOVA, Tukey post-hoc test. miR-146a ($F$ (1, 8) = 9.012, $P$ = 0.0170), Aβ/LPS ($F$ (1, 8) = 10.21, $P$ = 0.0127), miR-146a × Aβ/LPS ($F$ (1, 8) = 8.305, $P$ = 0.0205).
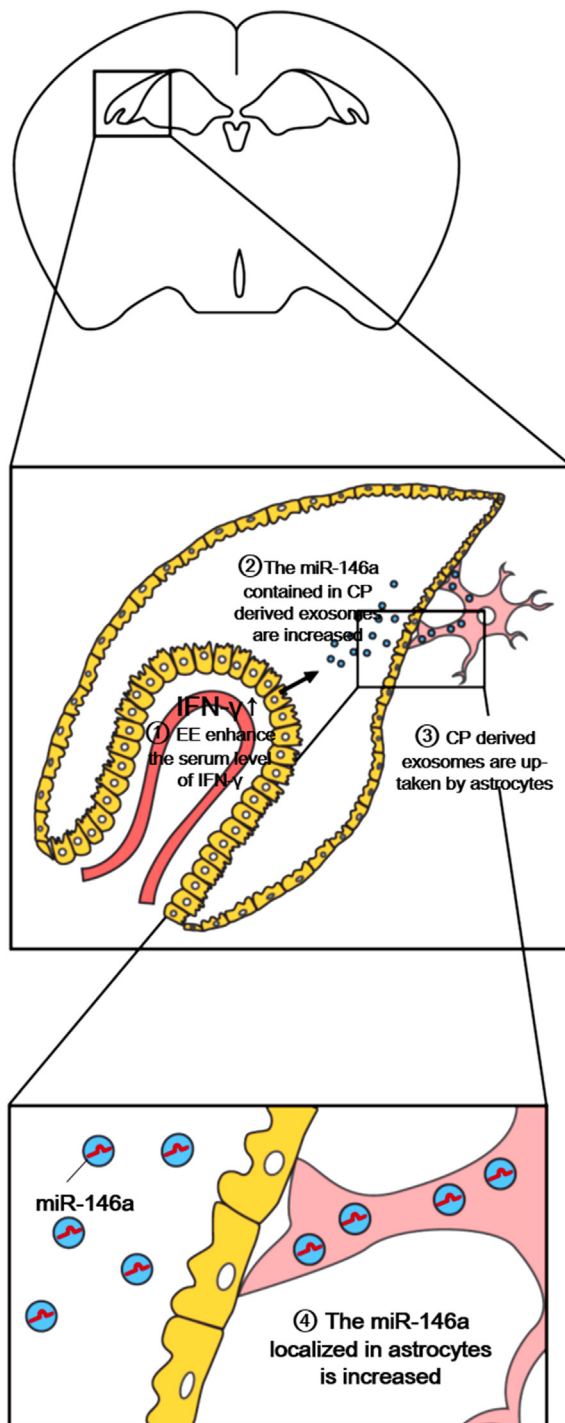
**Fig. 8. Schema of an EE.** The serum level of IFN-γ is up-regulated by an EE intervention, and IFN-γ stimulate the CP cells. Then, the miR-146a contained in CP derived exosomes are increased. After astrocytes up-take CP derived exosomes, the level of miR-146a localized in astrocytes is increased. The increased miR-146a act to suppress the inflammation of astrocytes in AD.

κB was calculated by dividing NF-κB positive area in nucleus by NF-κB positive area in cytoplasm. The nucleus/cytoplasm ratio of NF-κB was significantly increased in Aβ/LPS group compared to Control and Control + miR-146a group, and this increase was declined in Aβ/LPS + miR-146a group (Suppl. Fig. 9).

## 4. Discussion

To the best of our knowledge, this is the first report to show that an EE prevented cognitive impairment in AD model mice by stimulating CP cells. AD model mice treated with an EE showed increased synaptic density, down-regulated inflammation in astrocytes, even though the Aβ-positive area and neuronal number were unchanged. Surprisingly, up-regulated expression of miR-146a and down-regulated expression of NF-κB in the hippocampus were seen in AD model mice treated with an EE. The serum level of IFN-γ was up-regulated in EE-treated AD model mice, and IFN-γ enhanced the secretion of exosomal miR-146a from the CP. Finally, we found that the transfection of miR-146a into Aβ/LPS-treated astrocytes ameliorated the inflammatory state of astroglial cells. Thus, CP-derived exosomes are suggested to be key factors in suppressing the inflammation of reactive astrocytes, resulting in promotion of synaptogenesis and correction of cognitive impairment by an EE intervention.

We used 5 × FAD mice that carry five familial AD (FAD) mutations in amyloid precursor protein (APP) and presenilin 1 (PS1) transgenes and exhibit AD-like amyloidosis (Sasaguri et al., 2017). In an EE, animals are kept in a large group in a large cage with a running wheel and maze, so that they have frequent opportunities for social stimulation and voluntary physical activity (van Praag et al., 2000). In AD model mice, an EE is effective for improving cognitive impairment by enhancing synaptic plasticity, promoting neurogenesis, increasing brain-derived neurotropic factor, and reducing hippocampal oxidative stress (Hu et al., 2010; Polito et al., 2014; Prado Lima et al., 2018). In this study, both male and female of 5 × FAD mice showed preserved cognitive function by an EE. In addition, the cognitive function of WT/CC mice housed in 4 mice per cage was not different from WT/CC mice housed in 5–6 mice per cage. Thus the number of WT mice per CC cage might have no influence on the cognitive functions in this study.

In 5 × FAD mice, dense accumulation of Aβ was observed in the subiculum of the hippocampus, and an EE did not reduce the Aβ-positive area. Previously, we found that the severity of Aβ and tau accumulation is not associated with cognitive function, but synaptic density is correlated with dementia in a human post-mortem study (Kobayashi et al., 2018). Thus, factors other than Aβ accumulation seem to be associated with cognitive function in mice treated with an EE.

Immunohistochemistry showed significant reductions in the number of NeuN-positive neurons and synaptophysin intensity in 5 × FAD mice. An EE intervention did not alter the number of NeuN-positive cells in 5 × FAD mice, but both synaptophysin intensity and the number of synapses counted in the electron microscopic study were restored in mice exposed to EE. Because the intensity of synaptophysin was positively correlated with cognitive function, restoration of synaptic density by an EE intervention may have contributed to the improvement in cognitive function.

The effects of an EE on astrocytes were examined with GFAP staining. The number of GFAP-positive astrocytes and the GFAP-positive area were significantly increased in 5 × FAD mice. An EE intervention did not alter the number of astrocytes, but the GFAP-positive area was decreased. Because reactive astrocytes with increased expression of GFAP secrete inflammatory cytokines (Garwood et al., 2011; Pekny and Pekna, 2014) and impair synaptic plasticity (Finch, 2003), our data suggest that the reduction in the GFAP-positive area is associated with improvement in astrocytic function.

Additionally, the TNFα-positive area co-localized with GFAP was significantly increased in 5 × FAD mice, whereas this increase was down-regulated by an EE. An EE is known to reduce apolipoprotein E in reactive astrocytes and attenuates neuroinflammation (Ruscher et al., 2009). Because the area of GFAP and TNFα was negatively correlated with cognitive function, ameliorated astroglial dysfunction may be a key factor for synaptogenesis and cognitive function.

The effects of an EE on microglia were examined with Iba1 staining. The number of Iba1-positive microglia, which includes both resting and activated microglia, was significantly increased in 5 × FAD mice. Because

the activated type of microglia is classified into two types, the pro-inflammatory M1 type that expresses MHC class II and the anti-inflammatory M2 type that expresses MMR (Orihuela et al., 2016). We evaluated the characteristics of the M1 and M2 type by staining for MHC class II and MMR, respectively. Both the number of the M1 and M2 type of microglia was significantly increased in 5 × FAD mice, and these increases were not ameliorated by an EE intervention. Therefore, microglial changes seemed not to be contribute the cognitive improvement by EE.

In this study, the expression of miR-146a in the hippocampus in 5 × FAD/CC mice was increased compared to WT/CC mice. miR-146a is known to be up-regulated and act as a negative feedback regulator of NF-κB when the inflammation induce the NF-κB activation (Iyer et al., 2012). In addition, miR-146a is also known to show higher level in the temporal cortex of AD patients (Alexandrov et al., 2014). Because 5 × FAD/CC mice exhibited an increase in miR-146a as well as an increase in NF-κB, the negative feedback regulation of miR-146a is suggested to not work well.

In addition to AD, miR-146a is known to be up-regulated in astrocytes in Down syndrome (Arena et al., 2017). In addition to astrocytes, the M1 type of microglia is also known to show higher expression of miR-146a compared to the M2 type (Cunha et al., 2016). However, the EE did not affect the numbers of the M1 and M2 microglia in AD model mice. By considering these findings and the previous studies (Arena et al., 2017; Cunha et al., 2016), the increased level of miR-146a seemed to be occurred in astrocytes in AD model mice treated with an EE. miR-146a is known to target IRAK1 and TRAF6, resulting in attenuation of NF-κB signaling (Iyer et al., 2012). In the present study, 5 × FAD mice treated with an EE showed an increase in miR-146a, decreased expression of IRAK1 and TRAF6, and normalized NF-κB and TNFα in the hippocampus, compared to 5 × FAD mice housed in CC. Therefore, the further up-regulation of miR-146a might be needed for the regulation of IRAK1, TRAF6 and NF-κB in astrocytes in EE treated 5 × FAD mice.

CP epithelial cells secrete exosomes, which contain miR-146a and are taken up into astrocytes (Balusu et al., 2016b; Grapp et al., 2013). Impaired function of the CP is associated with AD pathology (Balusu et al., 2016a). Thus, we considered that CP-derived exosomes may affect the level of miR-146a in the hippocampus.

In the EE experiment, the serum concentration of IFN-γ in the 5 × FAD/EE group was significantly higher than that in the 5 × FAD/CC group. An EE is known to increase the concentration of IFN-γ in the CP and serum (Qi et al., 2018), and IFN-γ has a protective effect on spine density and long-term potentiation (Qi et al., 2018). We investigated whether the increased level of serum IFN-γ enhances CP cells to secrete exosomal miR-146a. When recombinant IFN-γ was added to cultured CP cells, the exosomal miR-146a in CP-CM of the 0.5 ng/ml IFN-γ group was significantly higher than that of the 0 ng/ml IFN-γ group. Previously, the low level of IFN-γ in the CP area in AD model is known to decrease the CP gateway for trafficking of leukocytes that act as an immune surveillance in the CNS (Baruch et al., 2014, 2015). Leukocytes that traffic to the CNS include Foxp3+ regulatory T cells that produce interleukin (IL)-10, which act to ameliorate AD pathology (Baruch et al., 2015). In this study, no difference was found in the hippocampal expression of Foxp3 as well as IL-10 between the 5 × FAD/CC and 5 × FAD/EE group (Suppl. Fig. 10a and b). Thus, regulatory T cells may not be associated with prevention of cognitive impairment in this study. Additionally, there was no significant difference in exosomal miR-146a in serum between the 5 × FAD/CC and 5 × FAD/EE group (Suppl. Fig. 11). Therefore, the peripheral level of miR-146a seemed to not be associated with cognitive function in this study.

To mimic the pathological change in astrocytes in AD, we isolated and cultured hippocampal astrocytes obtained from rat neonates and added 1 μM Aβ fibrils and 250 ng/ml LPS (Cordle and Landreth, 2005) to them. Although the GFAP-positive area per cell was not increased by addition of Aβ/LPS, the percentage of the TNFα-positive area per cell was significantly increased in the Aβ/LPS group, suggesting that these astrocytes showed an inflammatory state similar to the *in vivo* AD model. Because the transfection of miR-146a attenuated the percentage of the TNFα-positive area per cell in the Aβ/LPS group, miR-146a seemed to be a key factor for regulation of inflammation.

Moreover, the transfection of miR-146a down-regulated the mRNA expression of TRAF6 and NF-κB as well as the nucleus/cytoplasm ratio of NF-κB in protein level. Since the inflammation is known to translocate the expression of NF-κB from cytoplasm to nucleus, the nucleus/cytoplasm ratio of NF-κB is up-regulated in inflammatory states (Patel et al., 2017). Therefore, the decreased nucleus/cytoplasm ratio of NF-κB in Aβ/LPS + miR-146a group seemed to show the ameliorated inflammatory state. Previously, intranasal administration of miR-146a agomir was known to ameliorate glial activation and improve cognitive impairment in an AD mouse model, by down-regulating IRAK1, TRAF6 and NF-κB (Mai et al., 2019). In addition, we previously reported that MSC derived exosomal miR-146a inhibits the astrocytic inflammation and promotes the cognitive function in and AD mice (Nakano et al., 2020). From these studies, an EE is suggested to prevent the cognitive impairment by increasing the expression of miR-146a and decreasing that of IRAK1, TRAF6 and NF-κB in astrocytes.

The CP has been mainly considered the locus of the blood–CSF barrier and the tissue that is responsible for secretion of CSF. However, other functions such as regulation of selective leukocyte trafficking (Baruch et al., 2015) and circadian clock oscillations (Myung et al., 2018) were recently reported. In AD patients, altered tight junctions of CP epithelial cells, reduced secretion of CSF and neurotrophins, and accumulation of toxic molecules inside the cells have been reported (Balusu et al., 2016a). In the present study, the expression of transthyretin (TTR) in the CP area was down-regulated in the 5 × FAD/CC group compared to the WT/CC group (Suppl. Fig. 12). TTR reflects the function of the CP cells and is down-regulated in the CP area in AD mice (Balusu et al., 2016a; Gon-zalez-Marrero et al., 2015). In the present study, the decreased expression of TTR in the 5 × FAD/CC group was recovered in the 5 × FAD/EE group (Suppl. Fig. 12). Thus, an EE treatment may enhance not only the secretion of exosomal miR-146a from the CP, but also ameliorate other dysfunctions of the CP. Although we did not examine other factors such as miR-155 (Balusu et al., 2016b) or folate (Grapp et al., 2013) that are contained in CP-derived exosomes, miR-146a might be one of key factors for ameliorating cognitive impairment.

The present study shows that enhancing the secretion of exosomal miR-146a from the CP might have prevented cognitive impairment in EE treated AD model mice (Fig. 8). Previously, an EE is reported to regulate multiple miRNAs in 3xTg-AD model mice (Barak et al., 2013), however they have not shown the involvement of reactive astrocytes (Yeh et al., 2011). In this study, we report the effect of an EE on the expression of miR-146a in 5 × FAD mice which show reactive astrocytes and the involvement of CP derived exosomes on astrocytes, for the first time. miR-146a is also known to exert a detrimental effect, because Sison et al. report that astrocyte derived miR-146a induces the motor neuron loss in a model of spinal muscular atrophy (Sison et al., 2017). However, our study suggests that miR-146a plays a critical role to prevent the cognitive impairment. In the present study, we found that an EE prevents the cognitive impairment of AD model mice without affecting the level of Aβ. These findings suggest that an environmental condition may be one of factors that affects the onset of AD. Revealing the underlying mechanism of an EE is expected to apply to the prevention or the treatment of AD in human.

## Author contributions

M.N. and M.F. designed the study and wrote the paper. S.H. helped the experiment of MWM test. K.K., E.K., T.C. and Y.S. contributed to the interpretation of data.

## Declaration of competing interest

The authors declare that they have no conflicts of interests.

## Acknowledgements

## Appendix A. Supplementary data

Supplementary data to this article can be found online at https://doi.org/10.1016/j.bbih.2020.100149.

## References

Alexandrov, P.N., Dua, P., Lukiw, W.J., 2014. Up-regulation of miRNA-146a in progressive, age-related inflammatory neurodegenerative disorders of the human CNS. Front. Neurol. 5, 181.

Arena, A., Iyer, A.M., Milenkovic, I., Kovacs, G.G., Ferrer, I., Perluigi, M., Aronica, E., 2017. Developmental expression and dysregulation of miR-146a and miR-155 in down's syndrome and mouse models of down's syndrome and alzheimer's disease. Curr. Alzheimer Res. 14, 1305–1317.

Balusu, S., Brkic, M., Libert, C., Vandenbroucke, R.E., 2016a. The choroid plexus-cerebrospinal fluid interface in Alzheimer's disease: more than just a barrier. Neural regeneration research 11, 534–537.

Balusu, S., Van Wonterghem, E., De Rycke, R., Raemdonck, K., Stremersch, S., Gevaert, K., Brkic, M., Demeestere, D., Vanhooren, V., Hendrix, A., Libert, C., Vandenbroucke, R.E., 2016b. Identification of a novel mechanism of blood-brain communication during peripheral inflammation via choroid plexus-derived extracellular vesicles. EMBO Mol. Med. 8, 1162–1183.

Barak, B., Shvarts-Serebro, I., Modai, S., Gilam, A., Okun, E., Michaelson, D.M., Mattson, M.P., Shomron, N., Ashery, U., 2013. Opposing actions of environmental enrichment and Alzheimer's disease on the expression of hippocampal microRNAs in mouse models. Transl. Psychiatry 3, e304.

Baruch, K., Deczkowska, A., David, E., Castellano, J.M., Miller, O., Kertser, A., Berkutzki, T., Barnett-Itzhaki, Z., Bezalel, D., Wyss-Coray, T., Amit, I., Schwartz, M., 2014. Aging. Aging-induced type I interferon response at the choroid plexus negatively affects brain function. Science 346, 89–93.

Baruch, K., Ron-Harel, N., Gal, H., Deczkowska, A., Shifrut, E., Ndifon, W., Mirlas-Neisberg, N., Cardon, M., Vaknin, I., Cahalon, L., Berkutzki, T., Mattson, M.P., Gomez-Pinilla, F., Friedman, N., Schwartz, M., 2013. CNS-specific immunity at the choroid plexus shifts toward destructive Th2 inflammation in brain aging. Proc. Natl. Acad. Sci. U.S.A. 110, 2264–2269.

Baruch, K., Rosenzweig, N., Kertser, A., Deczkowska, A., Sharif, A.M., Spinrad, A., Tsitsou-Kampeli, A., Sarel, A., Cahalon, L., Schwartz, M., 2015. Breaking immune tolerance by targeting Foxp3(+) regulatory T cells mitigates Alzheimer's disease pathology. Nat. Commun. 6, 7967.

Battle, T., Preisser, L., Marteau, V., Meduri, G., Lambert, M., Nitschke, R., Brown, P.D., Corman, B., 2000. Vasopressin V1a receptor signaling in a rat choroid plexus cell line. Biochem. Biophys. Res. Commun. 275, 322–327.

Bhaskaran, M., Mohan, M., 2014. MicroRNAs: history, biogenesis, and their evolving role in animal development and disease. Veterinary pathology 51, 759–774.

Carro, E., Spuch, C., Trejo, J.L., Antequera, D., Torres-Aleman, I., 2005. Choroid plexus megalin is involved in neuroprotection by serum insulin-like growth factor I. J. Neurosci. : the official journal of the Society for Neuroscience 25, 10884–10893.

Carro, E., Trejo, J.L., Spuch, C., Bohl, D., Heard, J.M., Torres-Aleman, I., 2006. Blockade of the insulin-like growth factor I receptor in the choroid plexus originates Alzheimer's-like neuropathology in rodents: new cues into the human disease? Neurobiol. Aging 27, 1618–1631.

Cordle, A., Landreth, G., 2005. 3-Hydroxy-3-methylglutaryl-coenzyme A reductase inhibitors attenuate beta-amyloid-induced microglial inflammatory responses. J. Neurosci. : the official journal of the Society for Neuroscience 25, 299–307.

Cunha, C., Gomes, C., Vaz, A.R., Brites, D., 2016. Exploring new inflammatory biomarkers and pathways during LPS-induced M1 polarization. Mediat. Inflamm. 2016, 6986175.

Deczkowska, A., Baruch, K., Schwartz, M., 2016. Type I/II interferon balance in the regulation of brain physiology and pathology. Trends Immunol. 37, 181–192.

Doody, R.S., Raman, R., Farlow, M., Iwatsubo, T., Vellas, B., Joffe, S., Kieburtz, K., He, F., Sun, X., Thomas, R.G., Aisen, P.S., Siemers, E., Sethuraman, G., Mohs, R., 2013. A phase 3 trial of semagacestat for treatment of Alzheimer's disease. N. Engl. J. Med. 369, 341–350.

Fan, Y., Xie, L., Chung, C.Y., 2017. Signaling pathways controlling microglia chemotaxis. Mol. Cell. 40, 163–168.

Finch, C.E., 2003. Neurons, glia, and plasticity in normal brain aging. Neurobiol. Aging 24 (Suppl. 1), S123–S127 discussion S131.

Garwood, C.J., Pooler, A.M., Atherton, J., Hanger, D.P., Noble, W., 2011. Astrocytes are important mediators of Abeta-induced neurotoxicity and tau phosphorylation in primary culture. Cell Death Dis. 2, e167.

Gonzalez-Marrero, I., Gimenez-Llort, L., Johanson, C.E., Carmona-Calero, E.M., Castaneyra-Ruiz, L., Brito-Armas, J.M., Castaneyra-Perdomo, A., Castro-Fuentes, R., 2015. Choroid plexus dysfunction impairs beta-amyloid clearance in a triple transgenic mouse model of Alzheimer's disease. Front. Cell. Neurosci. 9, 17.

Grapp, M., Wrede, A., Schweizer, M., Huwel, S., Galla, H.J., Snaidero, N., Simons, M., Buckers, J., Low, P.S., Urlaub, H., Gartner, J., Steinfeld, R., 2013. Choroid plexus transcytosis and exosome shuttling deliver folate into brain parenchyma. Nat. Commun. 4, 2123.

Hardy, J., Selkoe, D.J., 2002. The amyloid hypothesis of Alzheimer's disease: progress and problems on the road to therapeutics. Science 297, 353–356.

Hu, Y.S., Xu, P., Pigino, G., Brady, S.T., Larson, J., Lazarov, O., 2010. Complex environment experience rescues impaired neurogenesis, enhances synaptic plasticity, and attenuates neuropathology in familial Alzheimer's disease-linked APPswe/PS1DeltaE9 mice. Faseb. J. : official publication of the Federation of American Societies for Experimental Biology 24, 1667–1681.

Iyer, A., Zurolo, E., Prabowo, A., Fluiter, K., Spliet, W.G., van Rijen, P.C., Gorter, J.A., Aronica, E., 2012. MicroRNA-146a: a key regulator of astrocyte-mediated inflammatory response. PloS One 7, e44789.

Kobayashi, E., Nakano, M., Kubota, K., Himuro, N., Mizoguchi, S., Chikenji, T., Otani, M., Mizue, Y., Nagaishi, K., Fujimiya, M., 2018. Activated forms of astrocytes with higher GLT-1 expression are associated with cognitive normal subjects with Alzheimer pathology in human brain. Sci. Rep. 8, 1712.

Kubota, K., Nakano, M., Kobayashi, E., Mizue, Y., Chikenji, T., Otani, M., Nagaishi, K., Fujimiya, M., 2018. An enriched environment prevents diabetes-induced cognitive impairment in rats by enhancing exosomal miR-146a secretion from endogenous bone marrow-derived mesenchymal stem cells. PloS One 13, e0204252.

Logan, S., Pharaoh, G.A., Marlin, M.C., Masser, D.R., Matsuzaki, S., Wronowski, B., Yeganeh, A., Parks, E.E., Premkumar, P., Farley, J.A., Owen, D.B., Humphries, K.M., Kinter, M., Freeman, W.M., Szweda, L.I., Van Remmen, H., Sonntag, W.E., 2018. Insulin-like growth factor receptor signaling regulates working memory, mitochondrial metabolism, and amyloid-beta uptake in astrocytes. Molecular metabolism 9, 141–155.

Mai, H., Fan, W., Wang, Y., Cai, Y., Li, X., Chen, F., Chen, X., Yang, J., Tang, P., Chen, H., Zou, T., Hong, T., Wan, C., Zhao, B., Cui, L., 2019. Intranasal administration of miR-146a agomir rescued the pathological process and cognitive impairment in an AD mouse model. Mol. Ther. Nucleic Acids 18, 681–695.

Marques, F., Sousa, J.C., 2015. The choroid plexus is modulated by various peripheral stimuli: implications to diseases of the central nervous system. Front. Cell. Neurosci. 9, 136.

Muller, M., Kuiperij, H.B., Claassen, J.A., Kusters, B., Verbeek, M.M., 2014. MicroRNAs in Alzheimer's disease: differential expression in hippocampus and cell-free cerebrospinal fluid. Neurobiol. Aging 35, 152–158.

Myung, J., Schmal, C., Hong, S., Tsukizawa, Y., Rose, P., Zhang, Y., Holtzman, M.J., De Schutter, E., Herzel, H., Bordyugov, G., Takumi, T., 2018. The choroid plexus is an important circadian clock component. Nat. Commun. 9, 1062.

Nakano, M., Kubota, K., Kobayashi, E., Chikenji, T.S., Saito, Y., Konari, N., Fujimiya, M., 2020. Bone marrow-derived mesenchymal stem cells improve cognitive impairment in an Alzheimer's disease model by increasing the expression of microRNA-146a in hippocampus. Sci. Rep. 10, 10772.

Nakano, M., Nagaishi, K., Konari, N., Saito, Y., Chikenji, T., Mizue, Y., Fujimiya, M., 2016. Bone marrow-derived mesenchymal stem cells improve diabetes-induced cognitive impairment by exosome transfer into damaged neurons and astrocytes. Sci. Rep. 6, 24805.

Neuropathology, G., 2001. Pathological correlates of late-onset dementia in a multicentre, community-based population in england and wales. Neuropathology group of the medical Research council cognitive function and ageing study (MRC CFAS). Lancet 357, 169–175.

Oakley, H., Cole, S.L., Logan, S., Maus, E., Shao, P., Craft, J., Guillozet-Bongaarts, A., Ohno, M., Disterhoft, J., Van Eldik, L., Berry, R., Vassar, R., 2006. Intraneuronal beta-amyloid aggregates, neurodegeneration, and neuron loss in transgenic mice with five familial Alzheimer's disease mutations: potential factors in amyloid plaque formation. J. Neurosci. : the official journal of the Society for Neuroscience 26, 10129–10140.

Orihuela, R., McPherson, C.A., Harry, G.J., 2016. Microglial M1/M2 polarization and metabolic states. Br. J. Pharmacol. 173, 649–665.

Patel, H., McIntire, J., Ryan, S., Dunah, A., Loring, R., 2017. Anti-inflammatory effects of astroglial alpha 7 nicotinic acetylcholine receptors are mediated by inhibition of the NF-kappaB pathway and activation of the Nrf 2 pathway. J. Neuroinflammation 14, 192.

Pekny, M., Pekna, M., 2014. Astrocyte reactivity and reactive astrogliosis: costs and benefits. Physiol. Rev. 94, 1077–1098.

Polito, L., Chierchia, A., Tunesi, M., Bouybayoune, I., Kehoe, P.G., Albani, D., Forloni, G., 2014. Environmental enrichment lessens cognitive decline in APP23 mice without affecting brain sirtuin expression. J. Alzheim. Dis. : JAD 42, 851–864.

Prado Lima, M.G., Schimidt, H.L., Garcia, A., Dare, L.R., Carpes, F.P., Izquierdo, I., Mello-Carpes, P.B., 2018. Environmental enrichment and exercise are better than social enrichment to reduce memory deficits in amyloid beta neurotoxicity. In: Proceedings of the National Academy of Sciences of the United States of America, vol. 115, pp. E2403–e2409.

Qi, F., Zuo, Z., Hu, S., Xia, Y., Song, D., Kong, J., Yang, Y., Wu, Y., Wang, X., Yang, J., Hu, D., Yuan, Q., Zou, J., Guo, K., Xu, J., Yao, Z., 2018. An enriched environment restores hepatitis B vaccination-mediated impairments in synaptic function through IFN-gamma/Arginase 1 signaling. Brain Behav. Immun. 71, 116–132.

Querfurth, H.W., LaFerla, F.M., 2010. Alzheimer's disease. N. Engl. J. Med. 362, 329–344.

Ruscher, K., Johannesson, E., Brugiere, E., Erickson, A., Rickhag, M., Wieloch, T., 2009. Enriched environment reduces apolipoprotein E (ApoE) in reactive astrocytes and

attenuates inflammation of the peri-infarct tissue after experimental stroke. J. Cerebr. Blood Flow Metabol. : official journal of the International Society of Cerebral Blood Flow and Metabolism 29, 1796–1805.

Salloway, S., Sperling, R., Fox, N.C., Blennow, K., Klunk, W., Raskind, M., Sabbagh, M., Honig, L.S., Porsteinsson, A.P., Ferris, S., Reichert, M., Ketter, N., Nejadnik, B., Guenzler, V., Miloslavsky, M., Wang, D., Lu, Y., Lull, J., Tudor, I.C., Liu, E., Grundman, M., Yuen, E., Black, R., Brashear, H.R., 2014. Two phase 3 trials of bapineuzumab in mild-to-moderate Alzheimer's disease. N. Engl. J. Med. 370, 322–333.

Samanta, S., Rajasingh, S., Drosos, N., Zhou, Z., Dawn, B., Rajasingh, J., 2018. Exosomes: new molecular targets of diseases. Acta Pharmacol. Sin. 39, 501–513.

Sasaguri, H., Nilsson, P., Hashimoto, S., Nagata, K., Saito, T., De Strooper, B., Hardy, J., Vassar, R., Winblad, B., Saido, T.C., 2017. APP mouse models for Alzheimer's disease preclinical studies. EMBO J. 36, 2473–2487.

Schulte-Herbruggen, O., Hamker, U., Meske, V., Danker-Hopfe, H., Ohm, T.G., Hellweg, R., 2007. Beta/A4-Amyloid increases nerve growth factor production in rat primary hippocampal astrocyte cultures. Int. J. Dev. Neurosci. : the official journal of the International Society for Developmental Neuroscience 25, 387–390.

Sison, S.L., Patitucci, T.N., Seminary, E.R., Villalon, E., Lorson, C.L., Ebert, A.D., 2017. Astrocyte-produced miR-146a as a mediator of motor neuron loss in spinal muscular atrophy. Hum. Mol. Genet. 26, 3409–3420.

Sonobe, T., Chenuel, B., Cooper, T.K., Haouzi, P., 2015. Immediate and long-term outcome of acute H2S intoxication induced coma in unanesthetized rats: effects of methylene blue. PloS One 10, e0131340.

Stopa, E.G., Berzin, T.M., Kim, S., Song, P., Kuo-LeBlanc, V., Rodriguez-Wolf, M., Baird, A., Johanson, C.E., 2001. Human choroid plexus growth factors: what are the implications for CSF dynamics in Alzheimer's disease? Exp. Neurol. 167, 40–47.

van Praag, H., Kempermann, G., Gage, F.H., 2000. Neural consequences of environmental enrichment. Nat. Rev. Neurosci. 1, 191–198.

Weitzner, D.S., Engler-Chiurazzi, E.B., Kotilinek, L.A., Ashe, K.H., Reed, M.N., 2015. Morris water maze test: optimization for mouse strain and testing environment. JoVE, e52706. JoVE.

Yeh, C.Y., Vadhwana, B., Verkhratsky, A., Rodríguez, J.J., 2011. Early astrocytic atrophy in the entorhinal cortex of a triple transgenic animal model of Alzheimer's disease. ASN neuro 3, 271–279.